

Breakup of a nucleus with two weakly bound neutrons on a proton target: Single-scattering approximation

A. Deltuva

Centro de Física Nuclear da Universidade de Lisboa, P-1649-003 Lisboa, Portugal

(Received January 31, 2013)

Three- and four-cluster breakup reactions in the ^{16}C -proton scattering are studied using three-body core-neutron-neutron model for ^{16}C . Single-scattering approximation (SSA) of four-particle equations for transition operators is used to calculate three- and four-cluster breakup amplitudes at 200 and 300 MeV/nucleon energy near proton-neutron (pn) quasi free scattering (QFS) conditions. The differential cross section is sharply peaked at pn QFS point and decreases rapidly whenever kinematical conditions deviate from pn QFS. The accuracy of the SSA for the three-cluster breakup is estimated from a three-body model and is found to be as good as 6% at higher reaction energies in suitable angular regimes. Furthermore, under an additional approximation the three-cluster breakup amplitude factorizes into the pn transition operator and the overlap integral of two- and three-particle bound states. That approximation usually reduces the cross section, in some cases even up to 10%.

PACS numbers: 24.10.-i, 21.45.-v, 25.10.+s, 25.60.Gc

I. INTRODUCTION

The structure and properties of exotic short-living nuclei are usually studied through their reactions with stable targets. On the theoretical side, the reliability of the extracted information depends on the validity of the assumed interaction model and on the accuracy of the theoretical methods used to solve the respective few- or many-body problem. Among the standard tools for the analysis of breakup reactions are the distorted wave Born approximation, the eikonal approximation [1], time-dependent models [2], and the more sophisticated continuum-discretized coupled-channels (CDCC) method [3]. For reactions involving effective two-cluster systems like deuteron or one-neutron halo nuclei that are treated as three-body problems (two-cluster nucleus plus a target) also the exact Faddeev-type formalism [4, 5] in the momentum-space framework has successfully been applied. Within this approach, once numerically well-converged results are obtained, all discrepancies with the experimental data can be attributed to the shortcomings of the used three-body model. However, practical applications of the Faddeev-type formalism are limited so far to light projectiles and targets.

On the other hand, Faddeev-type calculations can be used to check the accuracy of the traditional approximate nuclear reaction methods. Indeed, the comparison [6] of Faddeev-type and CDCC results revealed that CDCC is a reliable method for deuteron-nucleus elastic scattering and breakup but fails for the breakup of a one-neutron halo nucleus, assumed to be a bound state of an inert nuclear core (A) and a neutron (n), on a proton (p) target. More specifically, the peaks of the differential cross section in energy and angular distributions of the core A are underpredicted by CDCC. Those peaks are due to pn quasi free scattering (QFS), i.e., only the neutron interacts with the proton and is knocked out from the (An) nucleus whereas the momentum and energy trans-

fers to the core A vanish and, as a consequence, the core keeps the velocity of the incoming beam. Thus, near the pn QFS the reaction dynamics is dominated by the pn interaction which is very difficult to describe well when the three-particle CDCC wave function is expanded using the nA bound and selected continuum states as done in standard CDCC (the transfer-to-continuum CDCC [7] is more successful, but so far it is only available for three-body systems).

For the same reason one may expect the failure of CDCC for the breakup of a core and two-neutron nucleus (Ann) on a proton target near pn QFS kinematics, especially at higher energies relevant for the analysis of present day and future experiments. Although four-body CDCC [8, 9] and eikonal approximation [1] calculations for breakup of two-neutron halo nuclei exist, to the best of our knowledge, they were not applied in the pn QFS regime. Furthermore, additional technical difficulties arise in CDCC if two-body bound states (An) exist [10]. On the other hand, the rigorous treatment of the four-particle scattering problem within the Faddeev-type framework was successfully performed only for the four-nucleon system so far [11, 12]. The extension of the Faddeev-type method to distinguishable particles and high energies is very difficult technical challenge, although in principle it may be feasible. On the other hand, such a huge effort may be unnecessary for the description of particular breakup reactions where the CDCC is expected to fail, i.e., for $p + (Ann)$ breakup near pn QFS kinematics. The studies of ^{11}Be breakup on a proton target at 200 MeV/nucleon reaction energy [13] around the pn QFS kinematics revealed that the single scattering approximation (SSA) reproduces quite accurately the results of the full Faddeev-type calculations for not too small neutron scattering angles. Thus, one may expect the SSA to be reasonable also in the four-particle system at similar kinematical conditions. We therefore aim at developing the four-particle SSA to

study the breakup reactions $p + (Ann) \rightarrow p + n + (An)$ and $p + (Ann) \rightarrow p + n + n + A$ at higher energies. The numerical results use $p + {}^{16}\text{C}$ reactions as example. Unfortunately, no experimental data is available. In the present work we will concentrate on theoretical aspects of the three-cluster breakup where one may create effective three-body model $p + (Bn) \rightarrow p + n + B$ with $B = (An)$. Physically such a model is inadequate for weakly bound (An) , but it allows to perform full three-body Faddeev-type calculations and, by comparing with the respective SSA, identify the kinematical regimes where the SSA is reasonable, and estimate its accuracy.

In Sec. II we derive the SSA for the breakup amplitudes. In Sec. III we describe the employed interaction model. We study the three-cluster breakup in Sec. IV and four-cluster breakup in Sec. V. Summary is given in Sec. VI.

II. BREAKUP AMPLITUDES

We consider the four-particle system interacting via short-range pairwise potentials v_j where j labels the respective pair. We do not calculate the four-particle wave function explicitly but work in the momentum-space and use the integral form of the scattering equations as proposed by Alt, Grassberger and Sandhas (AGS) [14]. The AGS equations are equivalent to the Faddeev-Yakubovsky equations [15] but are formulated for the four-particle transition operators $\mathcal{U}_{\sigma\rho}^{ji}$, i.e.,

$$\mathcal{U}_{\sigma\rho}^{ji} = (G_0 t_i G_0)^{-1} \bar{\delta}_{\sigma\rho} \delta_{ji} + \sum_{\gamma k} \bar{\delta}_{\sigma\gamma} U_{\gamma}^{jk} G_0 t_k G_0 \mathcal{U}_{\gamma\rho}^{ki}, \quad (1)$$

The components of the operators are distinguished by the two-cluster partition and by the three-cluster partition; 18 different combinations are possible. The two-cluster partitions, denoted by Greek letters, are either of 1+3 or 2+2 type. The three-cluster partitions, denoted by Latin letters, are of 2+1+1 type and therefore are fully characterized by the pair of particles in the composite cluster. Obviously, the pairs i, j and k must be internal to the respective two-cluster partitions, i.e., $i \subset \rho, j, k \subset \gamma$ and $j \subset \sigma$, whereas $\bar{\delta}_{\sigma\rho} = 1 - \delta_{\sigma\rho}$. The components $\mathcal{U}_{\sigma\rho}^{ji}$ with all allowed j and i describe the transition from the initial two-cluster partition ρ to the final two-cluster partition σ [16]. In our example of the $p + (Ann)$ scattering the initial two-cluster partition ρ is $p + (Ann)$ with three internal pairs, i.e., (nn) and twice (An) . Other two-cluster partitions of the 1+3 type are $A + (nnp)$ and twice $n + (npA)$ while those of the 2+2 type are $(pA) + (nn)$ and twice $(pn) + (An)$. Note that the components of the transition operators exist even if the particles in the corresponding cluster do not bind as in the case of $(pA) + (nn)$; those components contribute to breakup reactions.

The free resolvent at the available system energy E is given by

$$G_0 = (E + i0 - H_0)^{-1} \quad (2)$$

where H_0 is the kinetic energy operator. The two-particle transition operator

$$t_j = v_j + v_j G_0 t_j \quad (3)$$

sums up the interactions for pair j up to all orders. Furthermore, all interactions within each two-cluster subsystem γ lead to the respective subsystem transition operators

$$U_{\gamma}^{jk} = G_0^{-1} \bar{\delta}_{jk} + \sum_i \bar{\delta}_{ji} t_i G_0 U_{\gamma}^{ik}. \quad (4)$$

As derived in Ref. [17], the amplitude for the three-cluster breakup of the initial two-cluster state is

$$\langle \Phi_j | T_{j\rho} | \Phi_{\rho} \rangle = \sum_{\gamma ki} \langle \Phi_j | U_{\gamma}^{jk} G_0 t_k G_0 \mathcal{U}_{\gamma\rho}^{ki} | \phi_{\rho}^i \rangle. \quad (5)$$

The energy parameter in the operators of Eq. (5) is $E = \epsilon_{\rho} + p_{\rho}^2/2\mu_{\rho}$ with ϵ_{ρ} being the energy of the bound state in the partition ρ and μ_{ρ} being the respective two-cluster reduced mass. The initial asymptotic channel state $|\Phi_{\rho}\rangle$ is a product of the bound state wave function in the partition ρ and the plane wave with momentum \mathbf{p}_{ρ} between the two clusters. $|\Phi_{\rho}\rangle = \sum_i |\phi_{\rho}^i\rangle$ is decomposed into its Faddeev components satisfying

$$|\phi_{\rho}^i\rangle = G_0 \sum_j \bar{\delta}_{ij} t_j |\phi_{\rho}^j\rangle \quad (6)$$

and normalized such that $\langle \Phi_{\sigma} | \Phi_{\rho} \rangle = \delta_{\sigma\rho} \delta(\mathbf{p}_{\sigma} - \mathbf{p}_{\rho})$. The asymptotic three-cluster state $|\Phi_j\rangle$ is an eigenstate of the channel Hamiltonian $H_0 + v_j$ with the eigenvalue E . It is given by the bound state wave function for the pair j times two plane waves corresponding to the relative motion of three free clusters.

The amplitude for the four-cluster breakup is taken over from Ref. [18], i.e.,

$$\langle \Phi_0 | T_{0\rho} | \Phi_{\rho} \rangle = \sum_{\gamma jki} \langle \Phi_0 | t_j G_0 U_{\gamma}^{jk} G_0 t_k G_0 \mathcal{U}_{\gamma\rho}^{ki} | \phi_{\rho}^i \rangle. \quad (7)$$

The four-cluster channel state $|\Phi_0\rangle$ is an eigenstate of H_0 with eigenvalue E ; it is a product of three plane waves (each is normalized to the Dirac δ -function) corresponding to the relative motion of four free particles.

In the SSA, i.e., keeping only the terms of the first order in two-particle transition operators (3), the three- and four-cluster breakup amplitudes become

$$\langle \Phi_j | T_{j\rho}^{\text{SSA}} | \Phi_{\rho} \rangle = \sum_k \bar{\delta}_{k\rho} \langle \Phi_j | t_k | \Phi_{\rho} \rangle, \quad (8a)$$

$$\langle \Phi_0 | T_{0\rho}^{\text{SSA}} | \Phi_{\rho} \rangle = \sum_k \bar{\delta}_{k\rho} \langle \Phi_0 | t_k | \Phi_{\rho} \rangle. \quad (8b)$$

Here $\bar{\delta}_{k\rho}$ is 0 if $k \subset \rho$ and 1 otherwise. Thus, in Eqs. (8) the summation runs over all pairs that are external to the initial state partition ρ . Note that Eq. (8a) is the amplitude for the direct three-cluster breakup and not

for rearrangement breakup, i.e., the final bound pair j is internal to the initial partition ρ .

In the following we consider the initial partition ρ to be of the 1+3 type, i.e., 1(234) with particle 1 as spectator and the bound state of particles (234). In such case the amplitudes (8) have three contributions $\sum_k \delta_{k\rho} t_k = t_{12} + t_{13} + t_{14}$ corresponding to the interactions of the spectator particle 1 with each particle in the cluster (234) but no interactions within the cluster.

We start with the four-cluster breakup amplitude (8b). Let m_a be the mass of the particle a and \mathbf{k}_a its final-state momentum with $a = 1, 2, 3, 4$. Furthermore, the initial momentum of particle 1 and of cluster (234) we denote by \mathbf{k}_1^i and \mathbf{k}_ρ^i , respectively. Obviously, \mathbf{k}_1^i , \mathbf{k}_ρ^i and \mathbf{k}_a are related by momentum and energy conservation, i.e., $\sum \mathbf{k}_a = \mathbf{k}_1^i + \mathbf{k}_\rho^i = \mathbf{K}$ and $\sum k_a^2/2m_a = \epsilon_\rho + k_1^{i2}/2m_1 + k_\rho^{i2}/2m_\rho = E$ with $m_\rho = m_2 + m_3 + m_4$. We do not assume a particular frame, thus, the results are valid with the energy E and momenta given in any frame. The explicit momentum-dependence of the t_{12} term is

$$\langle \Phi_0 | t_{12} | \Phi_\rho \rangle = \langle \mathbf{p}_{12} | t_{12}(e_{12} + i0) | \mathbf{p}'_{12} \rangle \langle \mathbf{q}_2 \mathbf{p}_{34} | \Phi_\rho \rangle \quad (9)$$

with

$$\mathbf{p}_{ab} = \frac{m_b \mathbf{k}_a - m_a \mathbf{k}_b}{m_a + m_b}, \quad (10a)$$

$$\mathbf{p}'_{1b} = \frac{m_b \mathbf{k}_1^i - m_1 \mathbf{k}'_b}{m_1 + m_b}, \quad (10b)$$

$$\mathbf{k}'_b = \mathbf{k}_1 + \mathbf{k}_b - \mathbf{k}_1^i, \quad (10c)$$

$$\mathbf{q}_2 = \frac{1}{m_\rho} [(m_3 + m_4) \mathbf{k}'_2 - m_2 (\mathbf{k}_3 + \mathbf{k}_4)]. \quad (10d)$$

Alternatively, another set of Jacobi momenta for the (234) subsystem could be chosen to represent $|\Phi_\rho\rangle$. Here and in the following the wave functions with notationally indicated momentum dependence refer to the internal motion of the respective bound cluster; the part corresponding to the free motion between clusters is taken out. The pair transition operator t_{12} depends on the energy available for the relative motion of particles 1 and 2, i.e.,

$$e_{12} = E - \frac{k_3^2}{2m_3} - \frac{k_4^2}{2m_4} - \frac{(\mathbf{k}_1 + \mathbf{k}_2)^2}{2(m_1 + m_2)}. \quad (11)$$

Due to momentum and energy conservation $e_{12} = p_{12}^2/2\mu_{12}$ with the reduced mass $\mu_{ab} = m_a m_b / (m_a + m_b)$; thus, the pair transition operator t_{12} has to be evaluated half-shell. Furthermore, although for brevity not explicitly indicated in our notation, the breakup amplitudes (8) and pair transition matrices (3) are operators in the spin-space implying summations over all intermediate spin states. In Eq. (9) this summation involves only the initial spin projection of the particle 2.

The momentum-dependence of the t_{13} and t_{14} terms has the same structure and can be easily obtained from Eq. (9) by the respective permutation of particle labels.

Considering the three-cluster breakup we assume that particles 3 and 4 build the final bound pair with mass $m_B = m_3 + m_4$, total momentum \mathbf{k}_B , internal wave function $\langle \mathbf{p}_{34} | \Phi_B \rangle$ and energy ϵ_B . The kinematics of the QFS condition for the pair of particles 1 and 2 reads $\mathbf{k}_B \approx \mathbf{k}_B^{\text{QFS}} = (m_B/m_\rho) \mathbf{k}_\rho^i$. The most important contribution of the breakup amplitude is the t_{12} term represented diagrammatically in Fig. 1 (a). It includes the interaction between the spectator and the struck particle,

$$\langle \Phi_B | t_{12} | \Phi_\rho \rangle = \int d^3 p_{34} [\langle \mathbf{p}_{12} | t_{12}(e_{12} + i0) | \mathbf{p}'_{12} \rangle \times \langle \Phi_B | \mathbf{p}_{34} \rangle \langle \mathbf{q}_2 \mathbf{p}_{34} | \Phi_\rho \rangle]. \quad (12)$$

The definitions of the involved momenta as given in Eqs. (10) are valid also here but $\mathbf{k}_3 = m_3 \mathbf{k}_B / (m_3 + m_4) + \mathbf{p}_{34}$ and $\mathbf{k}_4 = m_4 \mathbf{k}_B / (m_3 + m_4) - \mathbf{p}_{34}$ are not independent variables anymore. The momentum and energy conservation changes to $\mathbf{k}_1 + \mathbf{k}_2 + \mathbf{k}_B = \mathbf{k}_1^i + \mathbf{k}_\rho^i = \mathbf{K}$ and $\epsilon_B + k_1^2/2m_1 + k_2^2/2m_2 + k_B^2/2m_B = \epsilon_\rho + k_1^{i2}/2m_1 + k_\rho^{i2}/2m_\rho = E$. The energy e_{12} as defined in Eq. (11) is valid as well but it is more appropriate to express it via \mathbf{p}_{ab} , i.e.,

$$e_{12} = \frac{p_{12}^2}{2\mu_{12}} + \epsilon_B - \frac{p_{34}^2}{2\mu_{34}}. \quad (13)$$

Thus, this time the two-particle transition operator has to be evaluated fully off-shell. More importantly, Eq. (13) demonstrates that $t_{12}(e_{12} + i0)$ depends on the integration variable p_{34} and therefore cannot be taken out of the integral in Eq. (12). An additional approximation in the energy-dependence of t_{12} is needed to factorize the three-cluster breakup amplitude (12) into t_{12} and the overlap integral (OI)

$$\chi_\rho^B(\mathbf{q}_2) = \int d^3 p_{34} \langle \Phi_B | \mathbf{p}_{34} \rangle \langle \mathbf{q}_2 \mathbf{p}_{34} | \Phi_\rho \rangle. \quad (14)$$

We introduce the overlap integral approximation (OIA) of the three-cluster breakup amplitude as

$$\langle \Phi_B | T_{B\rho}^{\text{OIA}} | \Phi_\rho \rangle = \langle \mathbf{p}_{12} | t_{12} \left(\frac{p_{12}^2}{2\mu_{12}} + i0 \right) | \mathbf{p}'_{12} \rangle \chi_\rho^B(\mathbf{q}_2). \quad (15)$$

Under this particular approximation the two-particle transition operator needs to be evaluated half-shell only and the four-particle SSA becomes formally a three-particle SSA since the amplitude (15) has exactly the structure of the SSA breakup amplitude for the three-particle system (1+2+B) where the (2B) bound state wave function is replaced by the OI $\chi_\rho^B(\mathbf{q}_2)$.

The t_{13} and t_{14} terms of the three-cluster breakup amplitude (8a) have the structure diagrammatically represented in Fig. 1 (b). They include the interactions between the spectator and the particles that remain bound in the pair B, i.e.,

$$\langle \Phi_B | t_{13} | \Phi_\rho \rangle = \int d^3 p_{34} [\langle \mathbf{p}_{13} | t_{13}(e_{13} + i0) | \mathbf{p}'_{13} \rangle \times \langle \Phi_B | \mathbf{p}_{34} \rangle \langle \tilde{\mathbf{q}}_2 \tilde{\mathbf{p}}_{34} | \Phi_\rho \rangle] \quad (16)$$

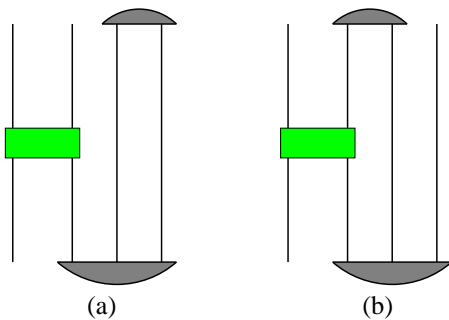


FIG. 1. (Color online) Two types of contributions to the three-cluster breakup amplitude in the SSA. The two-particle transition operator is represented by a box while two- and three-particle bound states are represented by filled arcs. The diagrams (a) and (b) correspond to Eqs. (12) and (16), respectively.

with $\tilde{\mathbf{q}}_2 = [(m_3 + m_4)\mathbf{k}_2 - m_2(\mathbf{k}'_3 + \mathbf{k}_4)]/m_\rho$, $\tilde{\mathbf{p}}_{34} = (m_4\mathbf{k}'_3 - m_3\mathbf{k}_4)/(m_3 + m_4)$, and e_{13} defined according to Eq. (11) with the permutation ($2 \leftrightarrow 3$). Thus, all relative momenta in Eq. (16) depend on the integration variable \mathbf{p}_{34} and therefore no simplifications are possible. However, our numerical calculations revealed that in the regime relevant for SSA, i.e., near pn QFS, the contributions of the type (16) are very small as compared to (12) and can be safely neglected. There are good physics reasons for this since, as mentioned, t_{13} and t_{14} terms describe the spectator interaction with the particles that form the bound pair B but not with the struck particle. The suppression of contribution (16) comes from high momentum components of the involved wave functions while in Eq. (12) low-momentum components are decisive.

For $p + (Ann)$ breakup reactions considered in this work two additional remarks regarding the symmetrization and the long-range Coulomb interaction are needed.

First, the channel states in Eqs. (8) have to be antisymmetric under exchange of the two neutrons. For the initial state $|\Phi_\rho\rangle$ this is achieved by including only antisymmetric two-neutron partial waves and keeping only two independent Faddeev components $|\phi_\rho^i\rangle$ when solving the three-particle bound state problem. The antisymmetrized final asymptotic three- and four-cluster states to be used in Eqs. (8) are

$$|\Phi_x^s\rangle = \frac{1}{\sqrt{2}}(1 - P_{nn})|\Phi_x\rangle \quad (17)$$

with P_{nn} being the two-neutron permutation operator. Since $|\Phi_\rho\rangle$ is already antisymmetrized and $t_{12} + t_{13} + t_{14}$ is symmetric under exchange of the neutrons, the antisymmetrization (17) simply yields an additional $\sqrt{2}$ factor for the amplitudes (8).

Second, the AGS equations for the transition operators are defined only with short-range potentials v_j . The Coulomb interaction (with no more than two charged

clusters) can be included using the method of screening and renormalization [19–21] but only in the full form of AGS equations where the unscreened limit for the renormalized amplitudes exists. This is not the case in the SSA: t_{pn} being Coulomb-free needs no renormalization while t_{pA} includes Coulomb and needs renormalization half-shell [19]. Thus, strictly speaking, their sum has no unscreened limit neither with nor without renormalization. Practically, this is not a problem since, according to our calculations, near the QFS conditions where the SSA is expected to be reasonable, the contribution of t_{pA} is very small and can safely be neglected.

III. INTERACTIONS

We take $p + {}^{16}\text{C} \rightarrow p + n + {}^{15}\text{C}$ and $p + {}^{16}\text{C} \rightarrow p + n + n + {}^{14}\text{C}$ reactions in inverse kinematics as a working example in the numerical calculations of this paper. The ground state of ${}^{14}\text{C}$, the core A, is well separated from the excited states (6.093 MeV) while ${}^{15}\text{C}$ is weakly bound ($\epsilon_B = -1.218$ MeV) one-neutron halo nucleus for which a simple two-body model of core A and neutron n is assumed to be adequate. The neutron separation energy of ${}^{16}\text{C}$ is 4.250 MeV such that core and two-neutron model of ${}^{16}\text{C}$ ground state 0^+ with $\epsilon_\rho = -5.468$ MeV appears to be quite reasonable.

As the pn and nn interactions we take the charge-dependent Bonn (CD Bonn) potential [22]. The nA interaction is taken over from Ref. [23]; it has central and spin-orbit parts of Woods-Saxon shape adjusted to ${}^{15}\text{C}$ bound states $2s_{1/2}$ and $1d_{5/2}$ and to ${}^{14}\text{C}$ neutron separation energy in $1p_{1/2}$. The deeply-bound Pauli forbidden states $1s_{1/2}$, $1p_{1/2}$, and $1p_{3/2}$ are projected out as described in Ref. [23]. The optical potential as parametrized by Koning & Delaroche [24] plus screened Coulomb is used for pA interaction; one could probably find a better parametrization but, as already mentioned, this is irrelevant since t_{pA} yields negligible contribution to SSA near pn QFS.

The above nn and nA potentials alone do not yield the desired value $\epsilon_\rho = -5.468$ MeV for the ${}^{16}\text{C}$ ground state. A simple way to remedy this shortcoming is to add a three-body force (3BF) acting in the nnA subsystem only. In this way it does not affect the functional form of the SSA breakup amplitudes (8). The coordinate-space calculations usually take a central 3BF depending on hyperradius. Our calculations are in momentum space so we take a central 3BF depending on hypermomentum \mathcal{K} that in the three-particle (234) subsystem has the form

$$\langle \mathbf{k}_2 \mathbf{k}_3 \mathbf{k}_4 | W | \mathbf{k}'_2 \mathbf{k}'_3 \mathbf{k}'_4 \rangle = (4\pi)^2 w_3 g(\mathcal{K}^2) g(\mathcal{K}'^2) \quad (18)$$

with $\mathcal{K}^2 = m_N[k_2^2/m_2 + k_3^2/m_3 + k_4^2/m_4 - (\mathbf{k}_2 + \mathbf{k}_3 + \mathbf{k}_4)^2/m_\rho]$ and \mathcal{K}'^2 defined analogously where m_N is the average nucleon mass. Note that $\mathcal{K}^2/2m_N$ is the internal motion kinetic energy of the (234) subsystem. We chose the form factor $g(\mathcal{K}^2) = \exp(-\mathcal{K}^2/2\Lambda^2)$ as Gaussian.

The form (18) of the 3BF is inspired by the effective field theory [25]. Once for each value of the cutoff parameter Λ the strength w_3 is adjusted to reproduce $\epsilon_\rho = -5.468$ MeV, the predictions become practically independent of Λ . For example, changing Λ by a factor of 2, from 2 fm^{-1} to 4 fm^{-1} , yields less than 3% changes in the breakup cross sections. Our standard choice is $\Lambda = 3 \text{ fm}^{-1}$.

With 3BF included the Faddeev components of the three-particle bound state obey the equation

$$|\phi_\rho^i\rangle = G_0 \sum_j \bar{\delta}_{ij} t_j |\phi_\rho^j\rangle + G_0(1 + t_i G_0) \eta_i W \sum_j |\phi_\rho^j\rangle \quad (19)$$

with $\sum \eta_i = 1$. Different η_i choices correspond to different splitting of the 3BF contributions among the Faddeev components but yield identical ϵ_ρ and $|\Phi_\rho\rangle$.

We calculate the two-particle transition operators t_j and the bound state wave functions $|\Phi_B\rangle$ and $|\Phi_\rho\rangle$ in the momentum-space partial-wave basis but then transform them into the plane-wave representation as needed in Eqs. (9-16). To obtain converged results the two-particle interactions v_j have to be included up to the two-particle relative orbital angular momentum L_{max}^j . We find that $L_{\text{max}}^j = 11$ for pn , 3 for nn , and 3 for nA is sufficient. The test calculations proving the negligible contribution of t_{pA} used $L_{\text{max}}^j = 20$.

We note that at $e_{12} = \epsilon_d$ with $\epsilon_d = -2.223$ MeV being the CD Bonn prediction for the deuteron bound state energy, the t_{pn} transition operator in the ${}^3S_1 - {}^3D_1$ partial wave exhibits the deuteron bound state pole. In the integrals it is treated by the subtraction technique.

IV. THREE-CLUSTER BREAKUP

We consider the three-cluster breakup where two clusters (a and b) are detected with momenta \mathbf{k}_a and \mathbf{k}_b (all single-cluster momenta in this section refer to the lab frame). The momentum of the undetected cluster c is fully determined by the momentum conservation. The energy conservation renders k_a and k_b not independent; for a fixed k_a there may be up to two solutions for k_b , and vice versa. The five independent kinematic variables for the fully exclusive fivefold differential cross section are often chosen as the polar and azimuthal scattering angles $\Omega_a = (\Theta_a, \varphi_a)$ and $\Omega_b = (\Theta_b, \varphi_b)$ of the two detected particles and one energy E_a , i.e.,

$$\frac{d^5\sigma}{d\Omega_a d\Omega_b dE_a} = \frac{(2\pi)^4 m_a m_b m_c k_a k_b^3}{V |(m_b + m_c)k_b^2 - m_b(\mathbf{K} - \mathbf{k}_a) \cdot \mathbf{k}_b|} \times \frac{1}{g_i} \sum_{m_s} |\langle \Phi_B | T_{B\rho} | \Phi_\rho \rangle|^2. \quad (20)$$

Here $V = |\mathbf{k}_1^i/m_1 - \mathbf{k}_\rho^i/m_\rho|$ is the incoming flux. The sum runs over all initial and final spin states, while $g_i = (2s_1+1)(2s_\rho+1)$ takes care of the spin averaging in initial state, s_1 (s_ρ) being the spin of the particle 1 (cluster ρ).

In our example of $p + {}^{16}\text{C} \rightarrow p + n + {}^{15}\text{C}$ reaction we assume that beam of ${}^{16}\text{C}$ is impinging on target p and the detected particles are ${}^{15}\text{C}$ in its ground state (B) and p . We compare the differential cross section (20) calculated in four different ways, depending on the scattering amplitude $\langle \Phi_B | T_{B\rho} | \Phi_\rho \rangle$. The four-particle SSA as given by Eqs. (12-13) is labeled SSA-4b. Its approximation (15) is labeled OIA-4b. The importance of higher order interactions between the three clusters can be estimated by creating an effective three-body model where the composite cluster B is treated as a single inert particle. The nB potential is real in 0^+ wave and supports bound state with energy $\epsilon_\rho - \epsilon_B$, while the pB interaction includes optical Koning & Delaroche [24] and Coulomb potentials; the latter is treated using the method of screening and renormalization [6, 20]. The results obtained by solving full three-body Faddeev-type equations, i.e., formally summing up multiple scattering (MS) series up to infinite order, are labeled MS-3b. The SSA of this model including only t_{pn} term is labeled SSA-3b. Although such model makes physically little sense owing to halo nature of B , but the ratio $[(\text{MS-3b}) - (\text{SSA-3b})]/(\text{MS-3b})$ should be a reasonable accuracy estimate of SSA-4b. Note that for comparison the results of the three-body model are multiplied by 2 to account for the two neutrons in the original four-particle model.

We concentrate on the kinematic regime near pn QFS, i.e., $\mathbf{k}_B \approx \mathbf{k}_B^{\text{QFS}} = (m_B/m_\rho)\mathbf{k}_\rho^i$. In terms of angles and energy this means $\Theta_B \approx 0$ and $E_B \approx E_B^{\text{QFS}} = (k_B^{\text{QFS}})^2/2m_B = (m_B/m_\rho)E_\rho^i$ where E_ρ^i is the beam energy of ${}^{16}\text{C}$. Note that at these conditions also \mathbf{q}_2 vanishes in Eq. (12).

In Fig. 2 we show the results at $E_\rho^i/16 = 300$ MeV. We fix $\Theta_B = 0^\circ$, $\varphi_B = 0^\circ$, $\varphi_p = 180^\circ$, and vary Θ_p . In all used approaches the differential cross section peaks quite sharply at (or very near to) $E_B = E_B^{\text{QFS}}$. This is due to sharp increase of the s -wave components of the bound state wave functions for vanishing relative momenta. At $\Theta_p = 15^\circ$ and 30° there is significant difference between MS-3b and SSA-3b indicating that the SSA is not reliable in this regime. On the contrary, at $\Theta_p = 45^\circ$ and 60° the agreement between MS-3b and SSA-3b gets better, of the order of 6% at the peak. Thus, for these kinematic configurations SSA-4b should be of a comparable accuracy. The SSA-4b results, taking into account the three-particle structure of ${}^{16}\text{C}$, are considerably lower than the ones of SSA-3b where this aspect is neglected. The OIA-4b, involving an additional approximation in the energy-dependence of t_{pn} , underestimates the SSA-4b up to 9%, most sizably at $\Theta_p = 45^\circ$.

In Fig. 3 we fix $\Theta_p = 45^\circ$ where the SSA is expected to be at its best but vary Θ_B and include also results for $E_\rho^i/16 = 200$ MeV. At this lower energy the difference between MS-3b and SSA-3b is more significant, around 15% at the peak while at $E_\rho^i/16 = 300$ MeV it remains below 10%. Thus, these results confirm once more that SSA is more reliable at higher energies. On

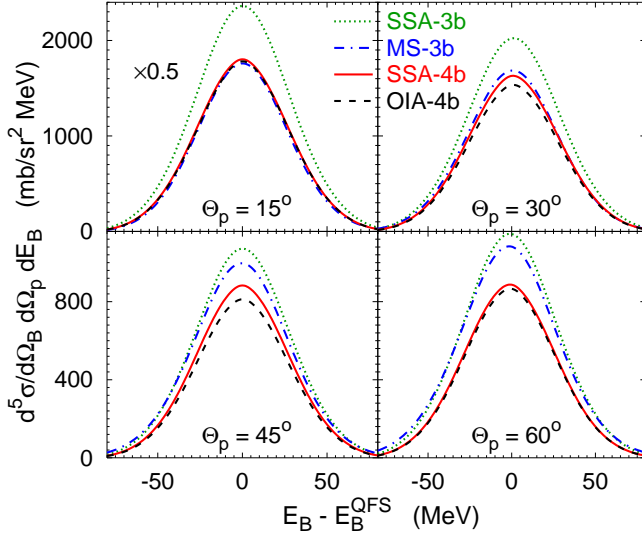


FIG. 2. (Color online) Differential cross section for $^{16}\text{C}(p, pn)^{15}\text{C}$ reaction in inverse kinematics as a function of the final ^{15}C energy E_B . The energy of the ^{16}C beam is 300 MeV/nucleon. ^{15}C and proton are detected at angles ($\Theta_B = 0^\circ, \varphi_B = 0^\circ$) and ($\Theta_p = 15, 30, 45, 60^\circ, \varphi_p = 180^\circ$). Results of SSA-3b (dotted), MS-3b (dotted-dashed), SSA-4b (solid) and OIA-4b (dashed) calculations are compared.

the other hand, sensitivity to the treatment of t_{pn} energy-dependence is slightly more pronounced at lower energies: the difference between SSA-4b and OIA-4b reaches 11% at $E_\rho^i/16 = 200$ MeV as compared to 9% at $E_\rho^i/16 = 300$ MeV. A further message from Fig. 3 is that at higher energy the differential cross section is more sharply peaked around the QFS point as it decreases faster with increasing Θ_B .

In Fig. 4 we show the results at $E_\rho^i/16 = 300$ MeV where a neutron is detected instead of a proton. As in Fig. 2 we fix $\Theta_B = 0^\circ, \varphi_B = 0^\circ, \varphi_n = 180^\circ$, and vary Θ_n . In this case the best agreement between MS-3b and SSA-3b, about 6%, is observed at intermediate angles $\Theta_n = 30^\circ$ and 45° while at $\Theta_n = 15^\circ$ and 60° the difference gets above 20%. The effect of OIA is most sizable at $\Theta_n = 45^\circ$ reaching 8%.

As can be concluded from the above results, the agreement between MS-3b and SSA-3b, i.e., the reliability of the SSA, depends not only on the reaction energy but also on the kinematical configuration. This dependence can be understood by inspecting the nB and pB relative energies in the final three-cluster breakup state, E_{nB} and E_{pB} . The values corresponding to QFS peaks in Fig. 2 are $E_{nB} = 258, 207, 137,$ and 66 MeV and $E_{pB} = 19, 70, 141,$ and 211 MeV for $\Theta_p = 15, 30, 45,$ and 60° , respectively. The values for Fig. 4 are obtained by simply interchanging E_{nB} and E_{pB} . Thus, the SSA appears to fail when either E_{nB} or E_{pB} is not large enough, with E_{pB} being more decisive, possibly due to pB Coulomb interaction. A detailed investigation of the MS-3b con-

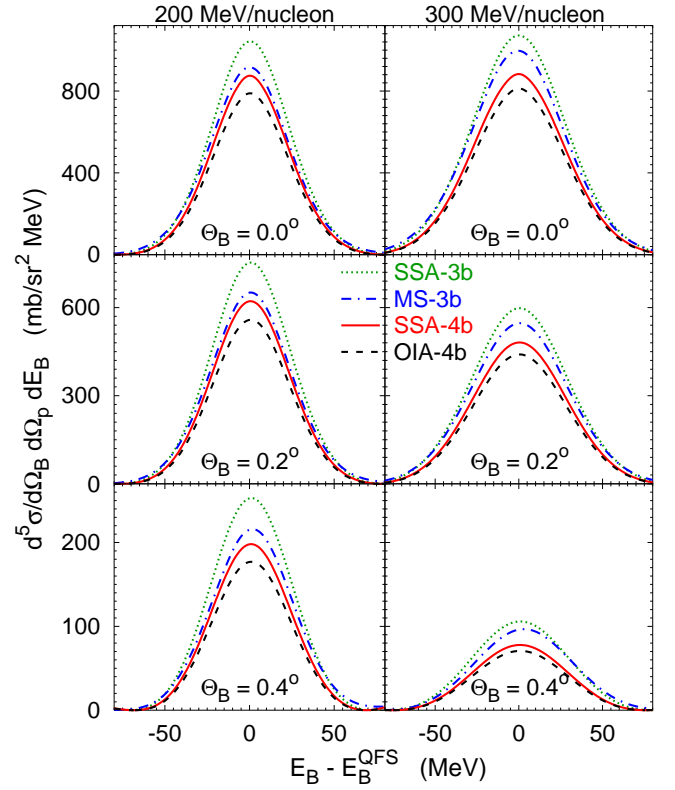


FIG. 3. (Color online) Same as Fig. 2 but for ^{16}C beam energy of 200 (left) and 300 (right) MeV/nucleon and scattering angles ($\Theta_B = 0.0, 0.2, 0.4^\circ, \varphi_B = 0^\circ$) and ($\Theta_p = 45^\circ, \varphi_p = 180^\circ$).

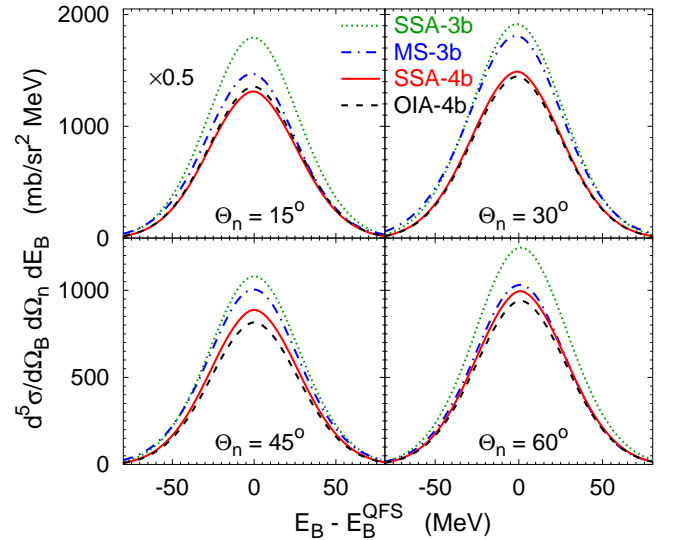


FIG. 4. (Color online) Same as Fig. 2 but a neutron is detected instead of a proton at angles ($\Theta_n = 15, 30, 45, 60^\circ, \varphi_n = 180^\circ$).

tributions reveals that, depending on E_{pB} and E_{nB} , its difference to SSA-3b is dominated by 2nd order terms $t_{pB}G_0t_{pn}$ or $t_{nB}G_0t_{pn}$.

We also note that at the QFS peaks the relative pn energy is around 150 MeV; thus, it is still in the regime where the underlying pn potential is well constrained by the experimental data.

The OIA as given by Eq. (15) results in higher values of the energy e_{12} at which the pn transition operator t_{pn} is evaluated as compared to the original SSA (13). This might lead to smaller t_{pn} values in OIA since the matrix elements of t_{pn} in average decrease with increasing energy much like the total pn cross section does. This may explain why the OIA-4b in most cases underestimates the SSA-4b predictions. Furthermore, we conjecture that the use of the overlap integrals in many-body reaction models would have qualitatively similar effect, i.e., would reduce the predicted cross sections.

V. FOUR-CLUSTER BREAKUP

A kinematically complete measurement of the four-cluster breakup requires the detection of three-clusters at least. As this is extremely difficult, semi-inclusive observables like momentum distributions are usually measured. Nevertheless, here we present results for the fully exclusive differential cross section that serves as an intermediate step for the calculation of semi-inclusive cross sections. With this goal in mind it is advantageous to choose the relative momenta as kinematical variables, i.e.,

$$\mathbf{k}_x = \frac{1}{2}(\mathbf{k}_{n_1} - \mathbf{k}_{n_2}), \quad (21a)$$

$$\mathbf{k}_y = \frac{2m_n\mathbf{k}_p - m_p(\mathbf{k}_{n_1} + \mathbf{k}_{n_2})}{m_p + 2m_n}, \quad (21b)$$

$$\mathbf{k}_z = \frac{(m_p + 2m_n)\mathbf{k}_A - m_A(\mathbf{k}_p + \mathbf{k}_{n_1} + \mathbf{k}_{n_2})}{M}, \quad (21c)$$

where the subscripts n_1 and n_2 distinguish between the two neutrons and $M = m_A + m_p + 2m_n$. The associated relative energies are $E_x = k_x^2/2\mu_x$, $E_y = k_y^2/2\mu_y$, and $E_z = k_z^2/2\mu_z$ with reduced masses $\mu_x = m_n/2$, $\mu_y = 2m_n m_p / (m_p + 2m_n)$, and $\mu_z = m_A(m_p + 2m_n)/M$. For example, \mathbf{k}_z and $E_z\mu_z/m_A$ are the momentum and energy of the nuclear core A in the four-particle center-of-mass (c.m.) system, while \mathbf{k}_x and E_x are the two-neutron relative momentum and energy. Owing to momentum and energy conservation there are eight independent kinematic variables; we choose them as the polar and azimuthal scattering angles $\Omega_j = (\Theta_j, \varphi_j)$ with $j = x, y, z$ and two energies E_x and E_z . In this representation the spin-averaged eightfold differential cross section is

$$\frac{d^8\sigma}{d\Omega_x d\Omega_y d\Omega_z dE_x dE_z} = \frac{(2\pi)^4}{V g_i} \sum_{m_s} |\langle \Phi_0 | T_{0\rho} | \Phi_\rho \rangle|^2 \times \mu_x \mu_y \mu_z k_x k_y k_z, \quad (22)$$

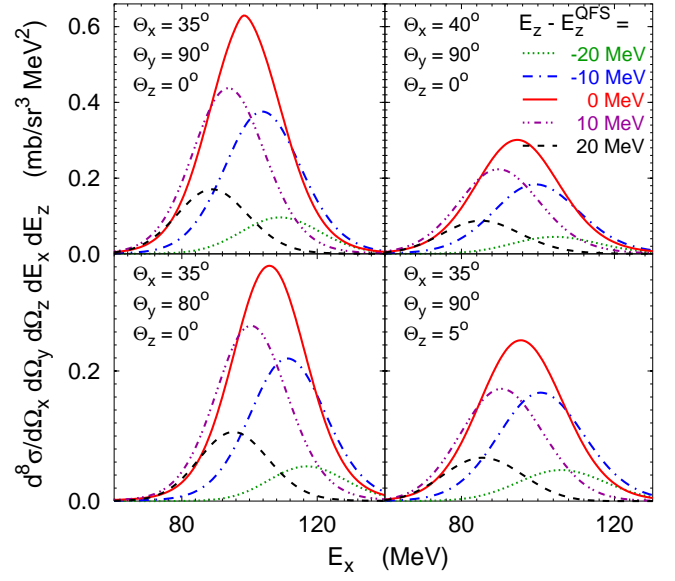


FIG. 5. (Color online) Differential cross section for $^{16}\text{C}(p, pnn)^{14}\text{C}$ reaction at $E_\rho^i/16 = 300$ MeV as a function of the relative nn energy E_x for selected values of E_z near pn QFS kinematics and angles Θ_x , Θ_y , and Θ_z whereas $\varphi_x = \varphi_y = \varphi_z = 0^\circ$.

where, as in Eq. (20), the sum runs over all initial and final spin states. The single-particle cross section for the core A in the c.m. frame can simply be obtained as

$$\frac{d^3\sigma_{\text{c.m.}}}{d\Omega_A dE_A} = \int d\Omega_x d\Omega_y dE_x \frac{m_A}{\mu_z} \frac{d^8\sigma}{d\Omega_x d\Omega_y d\Omega_z dE_x dE_z}. \quad (23)$$

The pn QFS implies $\mathbf{k}_A \approx \mathbf{k}_A^{\text{QFS}} = (m_A/m_\rho)\mathbf{k}_\rho^i$ and $\mathbf{k}_{n_2} \approx \mathbf{k}_{n_2}^{\text{QFS}} = (m_n/m_\rho)\mathbf{k}_\rho^i$ but also vanishing relative momentum $\mathbf{p}_{n_2A} = (m_A\mathbf{k}_{n_2} - m_n\mathbf{k}_A)/(m_A + m_n)$ and relative energy E_{n_2A} (here for simplicity we assume that n_1 is knocked out, but in practical calculations the amplitudes are antisymmetric with respect to the two neutrons). Thus, due to low relative nA energy the SSA is expected to be less accurate than for the three-cluster breakup in suitable kinematics. Nevertheless, in Fig. 5 we show the results for the fully exclusive differential cross section (22) of the $p + ^{16}\text{C} \rightarrow p + n + n + ^{14}\text{C}$ reaction at $E_\rho^i/16 = 300$ MeV. We fix the azimuthal angles $\varphi_x = \varphi_y = \varphi_z = 0^\circ$ and vary the polar angles near a pronounced QFS peak at $\Theta_x = 35^\circ$, $\Theta_y = 90^\circ$, and $\Theta_z = 0^\circ$. The cross section is shown as a function of the relative nn energy E_x for selected values of E_z around $E_z^{\text{QFS}} = [m_p^2 m_A^2 / (\mu_z m_\rho M^2)] E_\rho^i$. The results demonstrate that the differential cross section decreases rapidly whenever kinematical conditions deviate from QFS.

Finally, we note that the reliability of the SSA predictions for the semi-inclusive cross section (23) may be even more limited. The integration in Eq. (23) unavoidably includes regions of phase space with low relative pA energy where the higher order terms omitted in the SSA

may be significant.

VI. SUMMARY

Starting with full four-particle AGS equations for the transition operators we derived three- and four-cluster breakup amplitudes in the single-scattering approximation. Numerical calculations were performed for ^{16}C breakup on a proton target with the ^{14}C core and two-neutron model for the ^{16}C nucleus. Breakup reactions at 200 and 300 MeV/nucleon energy near pn QFS conditions were studied. In the case of the three-cluster breakup an additional three-body model, although being physically inadequate, allowed to estimate the accuracy of the SSA and thereby identify the kinematical regimes where the SSA is reliable. These regimes correspond to higher reaction energies and to higher relative energies between the composite cluster and any of the nucleons and are realized at proton or neutron scattering angles around 45° . There the accuracy of the SSA becomes as good as 6%. Furthermore, we have shown that an additional approximation in the energy dependence of the pn transition operator is needed to factorize the SSA of the three-cluster breakup amplitude into t_{pn} and the overlap

integral of two- and three-particle bound states. This approximation usually reduces the cross section, in some cases even up to 10%.

No SSA reliability test was possible for the four-cluster breakup but, given the conclusions drawn in the three-cluster case, it is expected to be less accurate. An extension of the present calculations to include also the double-scattering terms, especially those between the core and neutron at low relative energy, would be highly desirable.

The obtained three- and four-cluster breakup results demonstrate that the differential cross section is sharply peaked at pn QFS point and decreases rapidly whenever kinematical conditions deviate from pn QFS.

The present numerical calculations are limited to $p + ^{16}\text{C}$ reactions. However, the formalism is applicable also to other nuclei like ^{12}Be , ^{20}C , and ^{24}O , and, in the case of the four-cluster breakup, also to ^6He , ^{11}Li , and ^{22}C .

ACKNOWLEDGMENTS

The author thanks A. M. Moro for discussions and the Institute of Theoretical Physics and Astronomy of Vilnius University for its hospitality during the completion of this work. The work was partially supported by the FCT grant PTDC/FIS/65736/2006.

-
- [1] D. Baye, P. Capel, P. Descouvemont, and Y. Suzuki, Phys. Rev. C **79**, 024607 (2009).
 - [2] H. Esbensen, G. F. Bertsch, and C. A. Bertulani, Nucl. Phys. **A581**, 107 (1995).
 - [3] N. Austern, Y. Iseri, M. Kamimura, M. Kawai, G. Rawitscher, and M. Yahiro, Phys. Rep. **154**, 125 (1987).
 - [4] L. D. Faddeev, Zh. Eksp. Teor. Fiz. **39**, 1459 (1960) [Sov. Phys. JETP **12**, 1014 (1961)].
 - [5] E. O. Alt, P. Grassberger, and W. Sandhas, Nucl. Phys. **B2**, 167 (1967).
 - [6] A. Deltuva, A. M. Moro, E. Cravo, F. M. Nunes, and A. C. Fonseca, Phys. Rev. C **76**, 064602 (2007).
 - [7] A. M. Moro and F. M. Nunes, Nucl. Phys. **A767**, 138 (2006).
 - [8] T. Matsumoto, T. Egami, K. Ogata, Y. Iseri, M. Kamimura, and M. Yahiro, Phys. Rev. C **73**, 051602 (2006).
 - [9] M. Rodríguez-Gallardo, J. M. Arias, J. Gómez-Camacho, A. M. Moro, I. J. Thompson, and J. A. Tostevin, Phys. Rev. C **80**, 051601 (2009).
 - [10] A. M. Moro, private communication.
 - [11] A. Deltuva and A. C. Fonseca, Phys. Rev. C **86**, 011001(R) (2012).
 - [12] R. Lazauskas, Phys. Rev. C **86**, 044002 (2012).
 - [13] R. Crespo, A. Deltuva, E. Cravo, M. Rodríguez-Gallardo, and A. C. Fonseca, Phys. Rev. C **77**, 024601 (2008).
 - [14] P. Grassberger and W. Sandhas, Nucl. Phys. **B2**, 181 (1967); E. O. Alt, P. Grassberger, and W. Sandhas, JINR report No. E4-6688 (1972).
 - [15] O. A. Yakubovsky, Yad. Fiz. **5**, 1312 (1967) [Sov. J. Nucl. Phys. **5**, 937 (1967)].
 - [16] A. Deltuva and A. C. Fonseca, Phys. Rev. C **75**, 014005 (2007).
 - [17] A. Deltuva, Few-Body Syst. (2012), DOI:10.1007/s00601-012-0477-0.
 - [18] A. Deltuva, Phys. Rev. A **85**, 012708 (2012).
 - [19] E. O. Alt and W. Sandhas, Phys. Rev. C **21**, 1733 (1980).
 - [20] A. Deltuva, A. C. Fonseca, and P. U. Sauer, Phys. Rev. C **72**, 054004 (2005).
 - [21] A. Deltuva and A. C. Fonseca, Phys. Rev. Lett. **98**, 162502 (2007).
 - [22] R. Machleidt, Phys. Rev. C **63**, 024001 (2001).
 - [23] A. Deltuva, Phys. Rev. C **79**, 054603 (2009).
 - [24] A. J. Koning and J. P. Delaroche, Nucl. Phys. **A713**, 231 (2003).
 - [25] H. W. Hammer and L. Platter, Eur. Phys. J. A **32**, 113 (2007).